International Journal of Mechanical, Industrial and Aerospace Sciences
ISSN: 2517-9950
Vol:5, No:9, 2011

Thermo-mechanical deformation behavior of functionally graded rectangular plates subjected to various boundary conditions and loadings

Mohammad Talha and B N Singh

Abstract—This paper deals with the thermo-mechanical deformation behavior of shear deformable functionally graded ceramic-metal (FGM) plates. Theoretical formulations are based on higher order shear deformation theory with a considerable amendment in the transverse displacement using finite element method (FEM). The mechanical properties of the plate are assumed to be temperature-dependent and graded in the thickness direction according to a power-law distribution in terms of the volume fractions of the constituents. The temperature field is supposed to be a uniform distribution over the plate surface (XY plane) and varied in the thickness direction only. The fundamental equations for the FGM plates are obtained using variational approach by considering traction free boundary conditions on the top and bottom faces of the plate. A C^0 continuous isoparametric Lagrangian finite element with thirteen degrees of freedom per node have been employed to accomplish the results. Convergence and comparison studies have been performed to demonstrate the efficiency of the present model. The numerical results are obtained for different thickness ratios, aspect ratios, volume fraction index and temperature rise with different loading and boundary conditions. Numerical results for the FGM plates are provided in dimensionless tabular and graphical forms. The results proclaim that the temperature field and the gradient in the material properties have significant role on the thermo-mechanical deformation behavior of the FGM plates.

Keywords—Functionally graded material, higher order shear deformation theory, finite element method, independent field variables.

I. Introduction

An advanced composite materials known as functionally graded material (FGM) have received an appreciable consideration in structural engineering design, especially when the materials are subjected to extremely high thermal loading. The material property of the FGM can be tailored to accomplish the specific demands in different engineering utilization to achieve the advantage of the properties of individual material. This is possible due to the material composition of the FGM changes sequentially in a preferred direction. The applicability of this material is that it eliminates the interface problem due to proficient and continuous change of material properties from one surface to the other [1] [2]. The thermo-mechanical deformation of FGM structures have attracted the attention of many researchers in the past few years in different engineering applications which include design of aerospace structures, heat engine components and nuclear power plants etc.

Mohammad Talha, PhD Student, is with the Department of Aerospace Engineering, Indian Institute of Technology (IIT), Kharagpur, INDIA, 721 302, e-mail: rsmtalha@aero.iitkgp.ernet.in

B N Singh, Associate Professor, is with the Department of Aerospace Engineering, Indian Institute of Technology (IIT), Kharagpur, INDIA, 721 302, e-mail: bnsingh@aero.iitkgp.ernet.in

The assessment of thermo-mechanical deformation behavior of functionally graded plate structures considerably depends on the plate model kinematics. A number of plate theories are available to analyze the deformations of composite plates. The foremost constraint of using the classical Kirchhoff plate theory (CLPT) is that it ignores transverse shear effects and consequently provides reasonable results for relatively thin plates [24]. To abstain the said complication, an earlier attempts were made by Reissner [3] and Mindlin [4]. However, a shear-correction factor is needed to eliminate the problem of a constant transverse shear stress distribution. This correction factor was obtained by comparing the results with an exact elasticity solution and generally it depends on various parameters such as boundary conditions, geometric parameters, and loading conditions. This classical Kirchhoff plate theory seems to be unreliable for analysis of the FGM plates, in which volume fractions of two or more constituent varies smoothly and continuously as a function of position in a pre-defined specifications. Due to the continuous variation of material properties in a preferred direction, the first order shear deformation theory (FSDT) and higher order shear deformation theory (HSDT) may be efficiently utilized in the analysis. However, many HSDT kinematics were proposed, notable among them are [5], [6], [7], [8]. The higher order theories assumes the in-plane displacements as a cubic expression of the thickness coordinate and the out-of-plane displacement to be constant.

Several authors have used FSDT and HSDT kinematics to analyze the deformation characteristics of FGM plates. For example, Reddy [9] presented the mathematical formulation in conjunction with finite element model, based on third order shear deformation theory for static and dynamic analysis of the FGM plates. Abrate [10] analyzed the problems of free vibrations, buckling, and static deflections of the FGM plates using CLPT, FSDT, and HSDT kinematics. Sang and Hwan [11] Investigated vibration and thermal postbuckling behaviors of the functionally graded plates with nonlinear temperature distribution. Lanhe [12] applied FSDT kinematics to derive the equilibrium and stability equations of a moderately thick FGM rectangular plate under thermal loads, with two types of thermal loading, uniform temperature rise and gradient through the thickness. Saidi and Jomehhzadeh [13] presented a new analytical method for bendingstretching analysis of thick FGM plates based on the FSDT or Mindlin plate theory. Sheng and Wang [14] investigated the effect of thermal load on vibration, buckling and dynamic stability of FGM cylindrical shells em-

bedded in an elastic medium, based on FSDT by considering rotary inertia and the transverse shear strains. Ferreira *et al.* [15] used FSDT and multiquadric radial basis functions to analyze the static deformations of a simply supported FGM plates. They derived the effective properties of the composite either by rule of mixtures or by the Mori-Tanaka scheme. Yang and Shen [16] analyzed the free and forced vibration analyses for initially stressed FGM plates in thermal environment with temperature dependent material properties. The formulations are based on Reddy's higher order shear deformation theory which includes the thermal effects due to uniform temperature variation. Qian *et al.* [17] analyzed the static and dynamic response of a simply supported square FGM plate by using compatible higher order shear and normal deformable plate theory and a meshless Petrov-Galerkin method. Efraim and Eisenberger [18] derived the equations of motion for annular plates by employing FSDT which includes the effect of shear deformations to accomplish vibration frequencies and modes for various combinations of boundary conditions.

Naei *et al.* [19] presented the buckling analysis of radially-loaded circular FGM plate with variable thickness. The finite-element method is used to determine the critical buckling load and the effects of thickness variation and Poisson's ratio are investigated by calculating the buckling load. Navazi and Haddadpour [20] analytically investigated the aero−thermoelastic stability margins of FGM panels in thermal environment by employing piston theory of aerodynamics to model quasi-steady aerodynamic loading. Reddy and Cheng [21] studied the harmonic vibration problem of FGM plates in terms of transfer matrix by means of a three-dimensional asymptotic approach. Nguyen *et al.* [22] proposed the FSDT model for modelling structures made of FGM materials using energy equivalence methods. Liew *et al.* [23] presented a continuum three dimensional Ritz formulation for the vibration analysis of homogeneous thick rectangular plate with arbitrary combinations of boundary conditions.

With the enhanced utility of these materials in many diversified engineering applications, it is essential to know the thermo-mechanical deformation behavior of functionally graded ceramic-metal plates under various loading and boundary conditions. Considering the above said viewpoint in mind, the objective of this investigation is to present a higher order shear deformation theory with a cubically varying in-plane displacements over the entire thickness and quadratically varying transverse displacement to ensure the effects of normal strain and its derivative in calculation of transverse shear strains. The material properties of the FGM plates are graded continuously in the thickness direction. The variation of the properties follows according to a simple power-law distribution in terms of the volume fractions of the constituent. The implementation of this theory is executed by using a suitable C^0 continuous isoparametric finite element, and the governing equations are obtained using the variational approach. The thermo-mechanical deformations behavior of the FGM plates are examined for different thickness ratios, the aspect ratios, temperature rise, for different volume fraction indices, loading and boundary conditions. The present accomplished results are compared with those available in the literature. The obtained results are presented in the form of tables and figures to show the parametric effect such as material properties, thickness ratios, aspect ratios, temperature fields, the loading and boundary conditions, which can be treated as a benchmark for further advanced research. These furnished results are significant from the point of view in the designing of thermal barrier materials.

II. Problem Formulation

A. Governing equations

A schematic diagram of the problem studied and the rectangular cartesian coordinate system used describe the thermo-mechanical deformations of the FGM plate are shown in Fig. 1. It is assumed that the material properties of FGM plate varies in the thickness direction only, such that the top surface ($z = h/2$) of the plate is ceramic rich, whereas the bottom surface ($z = -h/2$) is metal rich. The effective material properties at an arbitrary point within the structural domain, like Young's modulus E, Poisson's ratio ν, mass density ρ, thermal expansion coefficient α, of the functionally graded plate are the effective material properties P. These properties are position dependent and can be expressed as,

$$P = P_t V_t(z) + P_b V_b(z) \tag{1}$$

where P_t and P_b represents the temperature dependent properties of the top and bottom faces of the plate, respectively, and can be expressed as a function of temperature [25].

$$P = P_0(P_{-1}T^{-1} + 1 + P_1T^1 + P_2T^2 + P_3T^3) \tag{2}$$

where P_0, P_{-1}, P_1, P_2, and P_3 are the coefficients of temperature $T(K)$ and are exclusive to the constituent materials. $V_t(z)$ and $V_b(z)$ are defined as the volume fractions of the constituent of the top and bottom faces of the plates, respectively, and are related by

$$V_t(z) + V_b(z) = 1 \tag{3}$$

The effective properties of functionally graded material

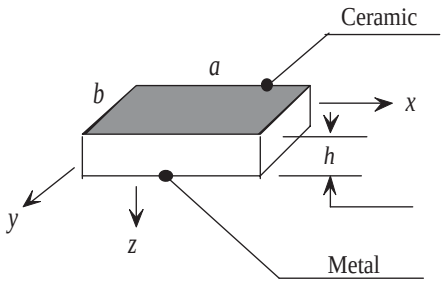

Fig. 1. Schematic diagram and dimensions of the plate.

are obtained according to a simple power−law. The volume fractions of the constituent of the top surface of the plate follows a simple power−law as,

$$V_t(z) = \left(\frac{2z+h}{2h}\right)^n \tag{4}$$

where n is the non-negative volume fraction index which prescribes the material variation profile through the thickness

of the plate and may be adjusted to obtain the optimum distribution of the constituent material. It is ascertained that the effective Young's modulus E and thermal expansion coefficient α are the temperature dependent. However, the mass density ρ and the thermal conductivity κ are independent of the temperature. Poisson's ratio ν is assumed to be constant as it weakly depends on the temperature changes. From Eqs. (1) and (4), the effective material properties with two constituents for graded plates can be expressed as,

$$\begin{array}{l} E(z,T) = [E_t(T) - E_b(T)]\left(\frac{2z+h}{2h}\right)^n + E_b(T) \\ \alpha(z,T) = [\alpha_t(T) - \alpha_b(T)]\left(\frac{2z+h}{2h}\right)^n + \alpha_b(T) \\ \rho(z) = (\rho_t - \rho_b)\left(\frac{2z+h}{2h}\right)^n + \rho_b \\ \kappa(z) = (\kappa_t - \kappa_b)\left(\frac{2z+h}{2h}\right)^n + \kappa_b \end{array} \tag{5}$$

Throughout the analysis the temperature field is applied in the thickness direction only and one-dimensional temperature field is assumed to be constant in the XY plane of the plate. In order to obtain the temperature distribution along the thickness a steady-state heat transfer equation is solved, and can be represented as

$$-\frac{d}{dz}\left[\kappa(z)\frac{dT}{dz}\right] = 0 \tag{6}$$

This equation is solved by prescribing boundary condition of $T = T_t$ at $z = h/2$ and $T = T_b$ at $z = -h/2$. It can be seen from Eqs. (5) and (7) that E_t, E_b, α_t and α_b are all functions of position and temperature dependent. The linear thermo-mechanical constitutive relations are,

$$\begin{Bmatrix} \sigma_{xx} \\ \sigma_{yy} \\ \sigma_{zz} \\ \sigma_{yz} \\ \sigma_{xz} \\ \sigma_{xy} \end{Bmatrix} = \begin{bmatrix} Q_{11} & Q_{12} & Q_{13} & 0 & 0 & 0 \\ Q_{12} & Q_{22} & Q_{23} & 0 & 0 & 0 \\ Q_{13} & Q_{23} & Q_{33} & 0 & 0 & 0 \\ 0 & 0 & 0 & Q_{44} & 0 & 0 \\ 0 & 0 & 0 & 0 & Q_{55} & 0 \\ 0 & 0 & 0 & 0 & 0 & Q_{66} \end{bmatrix} \times \left(\begin{Bmatrix} \varepsilon_{xx} \\ \varepsilon_{yy} \\ \varepsilon_{zz} \\ \gamma_{yz} \\ \gamma_{xz} \\ \gamma_{xy} \end{Bmatrix} - \begin{Bmatrix} 1 \\ 1 \\ 0 \\ 0 \\ 0 \\ 0 \end{Bmatrix} \alpha(z,T) \right) \tag{7}$$

where $\sigma_{xx}, \sigma_{yy}, \sigma_{zz}, \sigma_{xz}, \sigma_{yz}, \sigma_{xy}$ are the stress components, $\varepsilon_{xx}, \varepsilon_{yy}, \varepsilon_{zz}, \varepsilon_{xz}, \varepsilon_{yz}, \varepsilon_{xy}$ are the strain components. Q_{ij} are the stiffness coefficients, with $Q_{11} = Q_{22} = Q_{33} = \frac{E(z,T)(1-\nu^2)}{(1-3\nu^2-2\nu^3)}, Q_{12} = Q_{13} = Q_{23} = \frac{E(z,T)\nu(1+\nu)}{(1-3\nu^2-2\nu^3)}, Q_{44} = Q_{55} = Q_{66} = \frac{E(z,T)}{2(1+\nu)}$.

The linear strains corresponding to the displacements ($\bar{u}$, $\bar{v}$, $\bar{w}$) at any point along the (x, y, z) axes, respectively can be expressed as,

$$\begin{Bmatrix} \varepsilon_{xx} \\ \varepsilon_{yy} \\ \varepsilon_{zz} \\ \gamma_{yz} \\ \gamma_{xz} \\ \gamma_{xy} \end{Bmatrix} = \begin{bmatrix} \frac{\partial}{\partial x} & 0 & 0 \\ 0 & \frac{\partial}{\partial y} & 0 \\ 0 & 0 & \frac{\partial}{\partial z} \\ 0 & \frac{\partial}{\partial z} & \frac{\partial}{\partial y} \\ \frac{\partial}{\partial x} & 0 & \frac{\partial}{\partial x} \\ \frac{\partial}{\partial y} & \frac{\partial}{\partial z} & 0 \end{bmatrix} \begin{Bmatrix} \bar{u} \\ \bar{v} \\ \bar{w} \end{Bmatrix} \tag{8}$$

To incorporate the transverse shear effects in proposed HSDT kinematics, the displacement field is expressed in terms of mid-plane displacements u, v and w, perpendicular to mid-plane z, and the rotation of the normal ψ_x and ψ_y about the y and x-axis, respectively. In order to ensure the field variables to be continuous within the element for C^0 finite element modelling, the out of plane derivatives are considered as independent degrees of freedom, see [27] and the resulting modified displacement field is represented as,

$$\begin{array}{rcl} \bar{u} & = & u_0 + f_1(z)\psi_x + f_2(z)\alpha_x + f_3(z)\beta_x + f_4(z)\theta_x \\ \bar{v} & = & v_0 + f_1(z)\psi_y + f_2(z)\alpha_y + f_3(z)\beta_y + f_4(z)\theta_y \\ \bar{w} & = & w_0 + f_5(z)\psi_z + f_6(z)\alpha_z \end{array} \tag{9}$$

where $f_1(z) = C_1 z - C_2 z^3$, $f_2(z) = -C_3 z^2$, $f_3(z) = -C_4 z^3$, $f_4(z) = -C_5 z^3$, $f_5 = C_1 z$, $f_6 = C_1 z^2$, $C_1 = 1$, $C_2 = C_4 = 4/3h^2$, $C_3 = 1/2$, $C_5 = 1/3$ and $\xi_z = \alpha_z$. The basic field variables from the above equation is represented as:

$$\{q\} = \{u,\, v,\, w,\, \psi_x,\, \psi_y,\, \psi_z,\, \alpha_x,\, \alpha_y,\, \alpha_z,\, \beta_x,\, \beta_y,\, \theta_x,\, \theta_y\}^T \tag{10}$$

where, $\{q\}$ is named as displacement vector.

The strain vector terms in terms of mid-plane strain vector can be written as,

$$\begin{Bmatrix} \varepsilon_{xx} \\ \varepsilon_{yy} \\ \varepsilon_{zz} \\ \gamma_{yz} \\ \gamma_{xz} \\ \gamma_{xy} \end{Bmatrix} = \begin{Bmatrix} \varepsilon_1^0 \\ \varepsilon_2^0 \\ \varepsilon_3^0 \\ \varepsilon_4^0 \\ \varepsilon_5^0 \\ \varepsilon_6^0 \end{Bmatrix} + z \begin{Bmatrix} k_1^1 \\ k_2^1 \\ k_3^1 \\ k_4^1 \\ k_5^1 \\ k_6^1 \end{Bmatrix} + z^2 \begin{Bmatrix} k_1^2 \\ k_2^2 \\ 0 \\ k_4^2 \\ k_5^2 \\ k_6^2 \end{Bmatrix} + z^3 \begin{Bmatrix} k_1^3 \\ k_2^3 \\ 0 \\ 0 \\ 0 \\ k_6^3 \end{Bmatrix} \tag{11}$$

where,

$\varepsilon_1^0 = \frac{\partial u_0}{\partial x},\ \varepsilon_2^0 = \frac{\partial v_0}{\partial y},\ \varepsilon_3^0 = \psi_z,\ \varepsilon_4^0 = \psi_y + \frac{\partial w_0}{\partial y},\ \varepsilon_5^0 = \psi_x + \frac{\partial w_0}{\partial x}$,
$\varepsilon_6^0 = \frac{\partial u_0}{\partial y} + \frac{\partial v_0}{\partial x}\ k_1^1 = \frac{\partial \psi_x}{\partial x},\ k_2^1 = \frac{\partial \psi_y}{\partial y},\ k_3^1 = 2\alpha_z,$
$k_4^1 = \frac{\partial \psi_z}{\partial y} - \alpha_y,\ k_5^1 = \frac{\partial \psi_z}{\partial x} - \alpha_x,\ k_6^1 = \frac{\partial \psi_x}{\partial y} + \frac{\partial \psi_y}{\partial x}$
$k_1^2 = -C_3 \frac{\partial \psi_x}{\partial x},\ k_2^2 = -C_3 \frac{\partial \alpha_y}{\partial y},\ k_4^2 = \frac{\partial \alpha_z}{\partial y} - \theta_y - 3C_2(\psi_y + \beta_y),$
$k_5^2 = \frac{\partial \alpha_z}{\partial x} - \theta_x - 3C_2(\psi_x + \beta_x) k_6^2 = -C_3 \left(\frac{\partial \alpha_x}{\partial y} + \frac{\partial \alpha_y}{\partial x}\right),$
$k_1^3 = -C_2 \left(\frac{\partial \psi_x}{\partial x} + \frac{\partial \beta_x}{\partial x}\right) - C_5 \frac{\partial \theta_x}{\partial x},\ k_2^3 = -C_2 \left(\frac{\partial \psi_y}{\partial y} + \frac{\partial \beta_y}{\partial y}\right)$
$-C_5 \frac{\partial \theta_y}{\partial y} k_6^3 = -C_2 \left(\frac{\partial \psi_x}{\partial y} + \frac{\partial \psi_y}{\partial x} + \frac{\partial \beta_x}{\partial y} + \frac{\partial \beta_y}{\partial x}\right) - C_5 \left(\frac{\partial \theta_x}{\partial y} + \frac{\partial \theta_y}{\partial x}\right)$

In the above expressions, the terms having superscripts '0', '1' and '$2-3$' are membrane, curvature and higher order strain terms, respectively. The modulus E, thermal expansion

coefficient α and the elastic coefficients Q_{ij} vary through the plate thickness according to the Eqs.(4) and (5). The total in-plane force resultants, moments and higher order moments produced due to temperature rise are defined as,

$$\{N^T\} = \left\{ \begin{array}{c} N_{xx} \\ N_{yy} \\ N_{xy} \end{array} \right\} = \int_{-h/2}^{h/2} \left\{ \begin{array}{c} \sigma_{xx} \\ \sigma_{yy} \\ \sigma_{xy} \end{array} \right\} dz,$$

$$\{M^T\} = \left\{ \begin{array}{c} M_{xx} \\ M_{yy} \\ M_{xy} \end{array} \right\} = \int_{-h/2}^{h/2} \left\{ \begin{array}{c} \sigma_{xx} \\ \sigma_{yy} \\ \sigma_{xy} \end{array} \right\} z dz$$

and

$$\{P^T\} = \left\{ \begin{array}{c} P_{xx} \\ P_{yy} \\ P_{xy} \end{array} \right\} = \int_{-h/2}^{h/2} \left\{ \begin{array}{c} \sigma_{xx} \\ \sigma_{yy} \\ \sigma_{xy} \end{array} \right\} z^3 dz \qquad (12)$$

The thermal force $\{N^T\}$, $\{M^T\}$ and moment resultants $\{P^T\}$ can also be represented as,

$$\begin{aligned} \{N^T\} &= \int_{-h/2}^{h/2} \{\beta\}\, \Delta T\, dz \\ \{M^T\} &= \int_{-h/2}^{h/2} \{\beta\}\, \Delta T z\, dz \\ \{P^T\} &= \int_{-h/2}^{h/2} \{\beta\}\, \Delta T z^3\, dz \end{aligned} \qquad (13)$$

where,

$$\{\beta\} = [Q]\{\alpha\} = \left\{ \begin{array}{c} (Q_{11} + Q_{12})\alpha \\ (Q_{12} + Q_{22})\alpha \\ 0 \end{array} \right\} \qquad (14)$$

As the plate is exposed to thermal environment, and subsequently produces in-plane stress resultants (N_{xx} N_{yy} and N_{xy}). Therefore, the work done by the in-plane forces produced due to temperature change produces out of plane displacement 'w' by using small deformation theory as,

$$W_{th} = \frac{1}{2} \int_A \left\{ \begin{array}{c} w,x \\ w,y \end{array} \right\} \left[\begin{array}{cc} N_{xx} & N_{xy} \\ N_{xy} & N_{yy} \end{array} \right] \left\{ \begin{array}{c} w,x \\ w,y \end{array} \right\} dA \qquad (15)$$

B. Strain energy

The strain energy of the FGM plate is given by,

$$U = \frac{1}{2} \int_v \{\varepsilon\}_i^T \{\sigma\}_i dV \qquad (16)$$

The global displacement field model as given by Eq.(8) may be represented as,

$$\{\bar{u}\} = [\bar{N}]\{q\} \qquad (17)$$

where $\{q\}$ is as defined in Eq. (10) and the function of thickness co-ordinate $[\bar{N}]$ is defined as,

$$[\bar{N}] = \left[\begin{array}{ccccccccccccc} 1 & 0 & 0 & f_1(z) & 0 & 0 & f_2(z) & 0 & 0 & f_3(z) & 0 & f_4(z) & 0 \\ 0 & 1 & 0 & 0 & f_1(z) & 0 & 0 & f_2(z) & 0 & 0 & f_3(z) & 0 & f_4(z) \\ 0 & 0 & 1 & 0 & 0 & f_5(z) & 0 & 0 & f_6(z) & 0 & 0 & 0 & 0 \end{array} \right] \qquad (18)$$

C. Work done due to external transverse load

The external work done due to the distributed transverse static load $p_0(x, y)$ can be expressed as,

$$W_{ext} = \frac{1}{2} \int_A p_0(x, y) w dA. \qquad (19)$$

III. Solution methodology

A. Finite element model

A nine noded isoparametric element is employed for finite element modeling. In the FEM the domain is discretized into a set of finite elements. Over each of the elements, the displacement vector and element geometry of the model is expressed by

$$\{q\} = \sum_{i=1}^{NN} N_i \{q\}_i \,;\; x = \sum_{i=1}^{NN} N_i x_i \,;\; y = \sum_{i=1}^{NN} N_i y_i \qquad (20)$$

where N_i is the interpolation function (shape function) for the i^{th} node, $\{q\}_i$ is the vector of unknown displacements for the i^{th} node, NN is the number of nodes per element and x_i and y_i are Cartesian coordinate of the i^{th} node.

1) Strain energy of the plate: The strain energy of the FGM plate is given by,

$$U = \sum_{e=1}^{NE} U^{(e)} \qquad (21)$$

here NE is number of elements used for messing the plate $U^{(e)}$ is the elemental strain energy which can be obtained using Eqs. (16) and (20) and expressed as,

$$U = \frac{1}{2} \sum_{e=1}^{NE} \{q\}^{T(e)} [K]^{(e)} \{q\}^{(e)} \qquad (22)$$

here $[K]^{(e)}$ and $\{q\}^{(e)}$ are defined as linear stiffness matrix and displacement vector for the eth element, respectively. Using finite element model (Eq.(15)), Eq.(20) may also be written as,

$$W_{th} = \sum_{e=1}^{NE} W^{(e)} = \sum_{e=1}^{NE} \{q\}^{T(e)} [K_g]^{(e)} \{q\}^{(e)} dA, \qquad (23)$$

where, $[K_g]^{(e)}$ is defined as the elemental geometric stiffness matrix for the eth element.

2) Work done due to external transverse load: The work done by external mechanical load $p_0(x, y)$ is given by

$$V = W_{ext} = \frac{1}{2} \int_A p_0(x, y) w dA. \qquad (24)$$

Using the finite element notation model, Eq. (19) may be written as,

$$V = \sum_{e=1}^{NE} V^{(e)} \qquad (25)$$

where, $V^{(e)} = \int_{A^{(e)}} \{q\}^T \{P\} dA = \{q\}^{(e)^T} \{P\}^{(e)}$
with $\{P\}^{(e)} = (0\,0\,p_0\,0\,0\,0\,0\,0\,0\,0\,0\,0)^{T(e)}$

TABLE I
TEMPERATURE-DEPENDENT MATERIAL COEFFICIENTS FOR METAL AND CERAMICS, FROM REF. [26].

Materials	Properties	P_0	P_{-1}	P_1	P_2	P_3	P (T=300K)
ZrO_2	E(Pa)	244.27e+9	0	-1.371e-3	1.214e-6	-3.681e-10	168.063e+9
	α(1/K)	12.766e-6	0	-1.491e-3	1.006e-5	-6.788e-11	18.591e-6
Ti-6Al-4V	E(Pa)	122.56e+9	0	-4.586e-4	0	0	105.698e+9
	α(1/K)	7.75788e-6	0	6.638e-4	-3.147e-6	0	6.941e-6
Si_3N_4	E(Pa)	348.43e+9	0	-3.070e-4	2.160e-7	-8.946e-11	322.02715e+9
	α(1/K)	5.8723e-6	0	9.095e-4	0	0	7.474e-6
SUS304	E(Pa)	201.04e+9	0	3.079e-4	-6.534e-7	0	207.7877e+9
	α(1/K)	12.330e-6	0	8.086e-4	0	0	15.321e-6

B. Governing Equation

The governing equation for thermo-mechanical deformations of the FGM plate can be derived using variational principle as:

$$[\bar{K}]\{q\} = \{F\} \tag{26}$$

with, $[\bar{K}] = [K + \gamma K_c] - [K_g]$.

where, [K], $[K_c]$, $[K_g]$, $\{q\}$, and $\{F\}$ are global linear stiffness matrix, global linear stiffness matrix arises due to constraints, global geometric stiffness matrix due to thermal load, global displacement vector, and force vector, respectively.

IV. NUMERICAL EXAMPLES AND DISCUSSION

The numerical results for thermo-mechanical deformations of the FGMs plate are computed using the proposed mathematical model in conjunction with FEM. A computer programme has been developed in MATLAB 7.5.0 (R2007b) environment. The validation and efficacy of the proposed algorithm is examined by comparing the results with those available in the literature. A nine noded Lagrange isoparametric element, with 13 degrees of freedom (DOFs) per node for the present HSDT model has been used for discretizing the plate. For the computation of results full integration schemes (3x3) are used for thick plates and selective integration schemes (2x2) for thin plates. Table 1 shows the temperature dependent properties of the FGMs constituents which have been used for the computation of the results throughout the study, unless specified otherwise. Fig. 2 shows the volume fraction of the ceramic phase through the dimensionless thickness. It is assumed that the materials are perfectly elastic throughout the deformation.

The boundary conditions used in the present analysis are as follows:

Simply supported:(SSSS)

$u_0 = w_0 = \psi_y = \alpha_x = \alpha_z = \beta_y = \theta_x = 0$, at $x = 0$ and a.

$v_0 = w_0 = \psi_x = \alpha_y = \alpha_z = \beta_x = \theta_y = 0$, at $y = 0$ and b.

Clamped:(CCCC)

$u_0 = v_0 = w_0 = \psi_x = \psi_y = \psi_z = \alpha_x = \alpha_y = \alpha_z = \beta_x = \beta_y = \theta_x = \theta_y = 0$, at $x = 0$, a and $y = 0$, b.

Clamped-Free: (CFCF)

$u_0 = v_0 = w_0 = \psi_x = \psi_y = \psi_z = \alpha_x = \alpha_y = \alpha_z = \beta_x = \beta_y = \theta_x = \theta_y = 0$, at $x = 0$, and $y = 0$.

$u_0 \neq v_0 \neq w_0 \neq \psi_x \neq \psi_y \neq \psi_z \neq \alpha_x \neq \alpha_y \neq \alpha_z \neq \beta_x \neq \beta_y \neq \theta_x \neq \theta_y \neq 0$, at $x = a$ and $y = b$.

Simply supported-clamped: (SCSC)

$u_0 = w_0 = \psi_y = \alpha_x = \alpha_z = \beta_y = \theta_x = 0$, at $x = 0$ and $y = 0$.

$u_0 = v_0 = w_0 = \psi_x = \psi_y = \psi_z = \alpha_x = \alpha_y = \alpha_z = \beta_x = \beta_y = \theta_x = \theta_y = 0$, at $x = a$, $y = b$.

Hinged: (HHHH)

$u_0 = v_0 = w_0 = \psi_y = \alpha_y = \beta_y = \theta_y = 0$, at $x = 0$ and a.

$u_0 = v_0 = w_0 = \psi_x = \alpha_x = \beta_x = \theta_x = 0$, at $y = 0$, and $y = b$.

Clamped-Hinged: (CHCH)

$u_0 = v_0 = w_0 = \psi_x = \psi_y = \psi_z = \alpha_x = \alpha_y = \alpha_z = \beta_x = \beta_y = \theta_x = \theta_y = 0$, at $x = 0$, and $y = 0$.

$u_0 = v_0 = w_0 = \psi_y = \alpha_y = \beta_y = \theta_y = 0$, at $x = a$ and $y = b$

here, a and b refers the length and with of the plate, respectively.

A. Convergence and Comparison study

To make certain the accuracy and proficiency of the present finite element formulation, two test examples have been analyzed for thermo-mechanical deformations of the FGM plates.

Example 1. We first consider the accuracy of the present finite element formulation by comparing the results with those given by Ferreira *et. al.* [15] which is based on the third order deformation plate theory and a meshless method. In this example, the analysis is performed on a square functionally graded plate simply supported at all its edges (SSSS) for side to thickness ratio $a/h = 5$, volume fraction index $n = 0, 0.5, 1.0, 2$, and ∞ with aspect ratio $a/b = 1$. Where h is the thickness of the plate as defined earlier. The top face of the plate is ceramic-rich, whereas the bottom face is metal-rich. The plate is comprised of metal (Aluminium) and Ceramic. The material properties are taken as $E_b = 70 \times 10^9$ N/m^2 and $\nu_b = 0.3$ for Aluminium, and $E_t = 151 \times 10^9$ N/m^2 and $\nu_t = 0.3$ for ceramic. The transverse displacement w, the thickness coordinate z and the pressure q applied on the top surface have been non-dimensionalized as follows: $\bar{w} = w/h$, $\bar{z} = z/h$ and $\bar{p} = p/E_c h^4$. The comparison of present results with Ferreira *et. al.* [15] are presented in Table 2 which shows the agreement between the two results is excellent. The results clearly show that the performance of the present formulation is very good in terms of solution accuracy and the rate of convergence with mesh refinement. Therefore, based on the convergence study, it is concluded that (5×5) mesh is acceptable for thermo-mechanical deformation behavior of the FGM plate.

TABLE II
COMPARISON OF THE PRESENT RESULTS WITH REF. [15] FOR A SIMPLY SUPPORTED (SSSS) SQUARE FGM PLATE SUBJECTED TO UNIFORM DISTRIBUTED LOAD.

Mesh size	Volume fraction index, n				
	ceramic	0.5	1	2	metal
Present(2×2)	0.0239	0.0300	0.0330	0.0358	0.0500
Present(3×3)	0.0274	0.0345	0.0381	0.0414	0.0573
Present(4×4)	0.0218	0.0264	0.0303	0.0329	0.0455
Present(5×5)	0.0201	0.0256	0.0287	0.0312	0.0431
Present(6×6)	0.0201	0.0256	0.0286	0.0312	0.0431
Ferreira *et al*. [15]	0.0205	0.0262	0.0294	0.0323	0.0443
% Difference	1.99	2.34	2.43	3.52	2.78

Example 2. In this example we consider the static deformations of thick FGM plate made of Aluminium (Al) and Silicon Carbide (SiC) by using higher-order shear and normal deformable plate theory and meshless local Petrov-Galerkin method given by Qian *et. al*. [17]. The top surface of the plate is assumed to be ceramic-rich, whereas the bottom surface is metal rich. The thickness to side ration (a/h) is taken as 0.2. The top surface of the plate is loaded by a normal pressure obtained by $q_0 \sin \pi x/a \sin \pi y/a$ and the bottom surface of the plate is assumed to be traction free. The material properties for Al and SiC are as follows:

Al: E_b = 70 GPa, ν_b = 0.3, ρ_b = 2702 kg/m^3,
SiC: E_t = 427 GPa, ν_t = 0.17, ρ_t = 3100 kg/m^3.

In this example the transverse displacement w and thickness coordinate z have been non-dimensionalized as: $\bar{w} = \frac{100E_m h^3}{12a^4(1-\nu_m^2)q_0}w$, $\bar{z} = \frac{2z}{h}$. The plate is simply supported (SSSS) at all its edges. The nondimensional centre deflections with volume fraction index n along with the figure layout are preferred as used in Ref. [17] for direct comparison. Again, a good agreement is observed between the two results as shown in Fig.3.

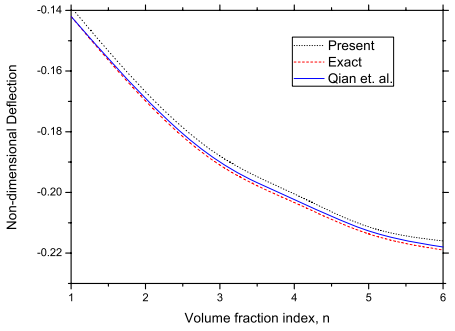

Fig. 2. Comparison of the present computed central deflection of an Al/SiC FGM plate with Qian *et. al*. [17].

These two comparison studies show that the present results matches well with the established one.

V. PARAMETRIC STUDIES

Based on the established approach and analyses of foregoing sections it is acknowledged that (5×5) mesh has been found to give good convergence for the FGM plates as mentioned earlier. These have been used for accomplishing the results, unless it is stated otherwise.

Table 3 shows the nondimensional central deflection of ZrO_2/Ti-6Al-4V square FGM plate in thermal environment. The analysis is performed for different values of volume fraction index n. The poisson's ratio for both the material is taken as 0.3 for simplicity and the side to thickness ratio is i.e., a/h=5. The top surface of the FGM plate is estimated to be ceramic-rich, whereas the bottom surface is metal rich. The various non-dimensionalized parameters used are: centre deflection, w/h; load parameter, $P = p_0 a^4/(E_b h^4)$; and thickness coordinate, $\bar{z} = z/h$. Here, p_0 denotes the intensity of the applied mechanical load, a, the side length of the plate, and h, the plate thickness. The isotropic ZrO_2 and Ti-6Al-4V cases resembles to a fully ceramic plate and a fully metallic plate, respectively, whereas the other cases (n = 0.5, 1, 10) are for the graded plates with two constituent materials. The temperature field is assumed to vary in the thickness direction only and is determined by the steady-state heat conduction equation along with the boundary conditions across the thickness of the plate. All plates are subjected to a uniform lateral pressure combined with a temperature rise $\Delta T = 100K$. It is found that, the isotropic ceramic plate has the lowest deflection for all the boundary conditions considered here, and the isotropic metallic has the largest deflection. Moreover, the deflections become higher with increasing n. This is due to the reality that the bending stiffness is the maximum for ceramic plate, while minimum for metallic plate, and degrades continuously as n increases. It is also found that the maximum deflection occurs for clamped-free (CFCF) boundary conditions and minimum for clamped (CCCC) boundary condition for all the cases considered here.

TABLE III
EFFECT OF VOLUME FRACTION INDEX n ON NONDIMENSIONAL CENTRAL DEFLECTION OF ZrO_2/TI-6AL-4V SQUARE FGM PLATE (A/H=5) SUBJECTED TO UNIFORM PRESSURE IN THERMAL ENVIRONMENT.

p_0	n	Boundary condition's					
		SSSS	CCCC	SCSC	CFCF	HHHH	CHCH
10	0	0.3689	0.1521	0.2240	0.9778	0.3778	0.2318
	0.5	0.4273	0.1753	0.2588	1.1345	0.4372	0.2676
	1	0.4547	0.1876	0.2765	1.2110	0.4655	0.2860
	10	0.5277	0.2209	0.3235	1.4016	0.5420	0.3354
	∞	0.5652	0.2334	0.3436	1.4982	0.5788	0.3556
20	0	0.7378	0.3041	0.4481	1.9556	0.7555	0.4636
	0.5	0.8546	0.3507	0.5177	2.2691	0.8744	0.5353
	1	0.9094	0.3753	0.5531	2.4219	0.9311	0.5720
	10	1.0554	0.4417	0.6471	2.8032	1.0840	0.6707
	∞	1.1304	0.4669	0.6873	2.9964	1.1576	0.7112
40	0	1.4755	0.6083	0.8961	3.9112	1.5110	0.9273
	0.5	1.7092	0.7013	1.0354	4.5382	1.7489	1.0705
	1	1.8187	0.7506	1.1061	4.8438	1.8622	1.1440
	10	2.1108	0.8835	1.2942	5.6064	2.1679	1.3415
	∞	2.2607	0.9338	1.3745	5.9927	2.3153	1.4224
100	0	3.6888	1.5207	2.2403	9.7781	3.7776	2.3182
	0.5	4.2730	1.7533	2.5885	11.3454	4.3722	2.6763
	1	4.5468	1.8764	2.7653	12.1096	4.6555	2.8599
	10	5.2770	2.2087	3.2354	14.0160	5.4198	3.3536
	∞	5.6518	2.3344	3.4363	14.9818	5.7882	3.5560

Table 4 represents the nondimensional central deflection of ZrO_2/Ti-6Al-4V square FGM plate subjected to a uniform lat-

TABLE IV
EFFECT OF VOLUME FRACTION INDEX n ON NONDIMENSIONAL CENTRAL DEFLECTION OF ZrO_2/Ti-6Al-4V SQUARE FGM PLATE (A/H=10) SUBJECTED TO UNIFORM PRESSURE IN THERMAL ENVIRONMENT.

p_0	n	Boundary condition's					
		SSSS	CCCC	SCSC	CFCF	HHHH	CHCH
10	0	0.3109	0.1030	0.1658	0.8127	0.3232	0.1721
	0.5	0.3616	0.1196	0.1928	0.9465	0.3755	0.1999
	1	0.3839	0.1276	0.2054	1.0085	0.3988	0.2130
	10	0.4409	0.1472	0.2363	1.1551	0.4595	0.2456
	∞	0.4758	0.1577	0.2538	1.2435	0.4946	0.2635
20	0	0.6219	0.2060	0.3316	1.6253	0.6464	0.3442
	0.5	0.7232	0.2393	0.3855	1.8931	0.7509	0.3999
	1	0.7679	0.2552	0.4107	2.0171	0.7976	0.4261
	10	0.8817	0.2944	0.4725	2.3101	0.9190	0.4913
	∞	0.9515	0.3154	0.5076	2.4871	0.9892	0.5270
40	0	1.2438	0.4120	0.6633	3.2506	1.2929	0.6885
	0.5	1.4463	0.4785	0.7711	3.7862	1.5018	0.7998
	1	1.5358	0.5104	0.8214	4.0341	1.5951	0.8521
	10	1.7634	0.5889	0.9451	4.6203	1.8380	0.9825
	∞	1.9031	0.6308	1.0152	4.9741	1.9785	1.0539
100	0	3.1094	1.0300	1.6582	8.1266	3.2322	1.7212
	0.5	3.6158	1.1963	1.9277	9.4654	3.7546	1.9994
	1	3.8394	1.2760	2.0536	10.0853	3.9878	2.1303
	10	4.4086	1.4722	2.3627	11.5507	4.5950	2.4564
	∞	4.7577	1.5771	2.5381	12.4353	4.9462	2.6348

TABLE V
EFFECT OF VOLUME FRACTION INDEX n ON NONDIMENSIONAL CENTRAL DEFLECTION OF ZrO_2/Ti-6Al-4V RECTANGULAR ($b = a$) FGM PLATE (A/H=5) SUBJECTED TO UNIFORM PRESSURE IN THERMAL ENVIRONMENT.

p_0	n	Boundary condition's					
		SSSS	CCCC	SCSC	CFCF	HHHH	CHCH
10	0	0.8417	0.2798	0.4497	2.5293	0.8796	0.4676
	0.5	0.9764	0.3229	0.5204	2.9409	1.0195	0.5408
	1	1.0376	0.3454	0.5555	3.1356	1.0841	0.5774
	10	1.1986	0.4051	0.6465	3.6066	1.2560	0.6735
	∞	1.2882	0.4290	0.6889	3.8707	1.3463	0.7165
20	0	1.6835	0.5595	0.8993	5.0587	1.7591	0.9352
	0.5	1.9528	0.6458	1.0408	5.8818	2.0390	1.0816
	1	2.0751	0.6908	1.1110	6.2712	2.1682	1.1548
	10	2.3972	0.8101	1.2931	7.2131	2.5121	1.3469
	∞	2.5764	0.8581	1.3777	7.7415	2.6925	1.4329
40	0	3.3670	1.1190	1.7986	10.1173	3.5182	1.8704
	0.5	3.9057	1.2917	2.0816	11.7637	4.0779	2.1632
	1	4.1502	1.3815	2.2219	12.5424	4.3364	2.3097
	10	4.7945	1.6202	2.5862	14.4263	5.0241	2.6938
	∞	5.1527	1.7162	2.7554	15.4830	5.3851	2.8659
100	0	8.4175	2.7976	4.4965	25.2934	8.7956	4.6760
	0.5	9.7642	3.2292	5.2041	29.4092	10.1948	5.4081
	1	10.3756	3.4538	5.5548	31.3560	10.8411	5.7742
	10	11.9861	4.0506	6.4654	36.0657	12.5604	6.7345
	∞	12.8818	4.2904	6.8886	38.7075	13.4627	7.1647

eral pressure combined with a uniform temperature rise $\Delta T = 100K$. The various non-dimensionalized parameters used are: centre deflection, w/h; load parameter, $P = p_0 a^4/(E_b h^4)$; and thickness coordinate, $\bar{z} = z/h$. The side to thickness ratio is (a/h) is taken as 10 and the uniform lateral pressure is ranging from q_0 = 10 to q_0 = 100. The nondimensional central deflection increases as the volume fraction index n increases in all type of boundary conditions considered here. This is expected, because a larger volume fraction index means that the plate has a smaller ceramic component, and that its stiffness is thus reduced. The variation of nondimensional central deflection of ZrO_2/Ti-6Al-4V rectangular FGM plate subjected to a uniform lateral pressure combined with a temperature rise $\Delta T = 100K$ is described in Tables 5 and 6 for a/h = 5 and 10, respectively. The thermo-mechanical deformation characteristics shown in these two tables are similar to those in tables 3 and 4. It is also evident that the rectangular plates deflected more than the square plates.

Table 7 shows the nondimensional central deflection of ZrO_2/Ti-6Al-4V FGM plate subjected to a sinusoidal load given by $q_0 \sin \pi x/a \sin \pi y/a$ combined with a temperature rise $\Delta T = 100K$ for various boundary conditions considered here. The side to thickness ratio (a/h) = 5 and the plate aspect ratio (b/a) is taken as 1 and 2, respectively. The transverse displacement w and thickness coordinate z have been non-dimensionalized as: $\bar{w} = \frac{100 E_m h^3}{12 a^4 (1-\nu_m^2) q_0} w$, $\bar{z} = \frac{2z}{h}$. The mass density and thermal conductivity are: ρ = 2370 kg/m^3, κ = 1.8W/mK for ZrO_2; ρ = 4429 kg/m^3, κ = 7.82W/mK for Ti-6Al-4V. Young's modulus and thermal expansion coefficient of theses materials are assumed to be temperature-dependent as given in Table 1. The load parameter p_0 is taken as unity. It is noticed that in the case of square plate (b/a=1) the maximum center deflection is found for simply supported (SSSS) boundary conditions and least for clamped (CCCC) boundary condition, whereas, for rectangular plate (b/a=2) maximum is found for clamped-free (CFCF) and minimum for clamped (CCCC) boundary condition. The nondimensional central deflection increases as the volume fraction index n increases in all type of boundary conditions considered here, as expected.

TABLE VI
EFFECT OF VOLUME FRACTION INDEX n ON NONDIMENSIONAL CENTRAL DEFLECTION OF ZrO_2/Ti-6Al-4V RECTANGULAR ($b = a$) FGM PLATE (A/H=10) SUBJECTED TO UNIFORM PRESSURE IN THERMAL ENVIRONMENT.

p_0	n	Boundary condition's					
		SSSS	CCCC	SCSC	CFCF	HHHH	CHCH
10	0	0.7546	0.2001	0.3567	2.2477	0.7836	0.3687
	0.5	0.8776	0.2325	0.4149	2.6200	0.9106	0.4287
	1	0.9311	0.2479	0.4418	2.7902	0.9665	0.4565
	10	1.0678	0.2853	0.5069	3.1872	1.1115	0.5248
	∞	1.1536	0.3061	0.5453	3.4368	1.1982	0.5639
20	0	1.5091	0.4002	0.7133	4.4954	1.5672	0.7374
	0.5	1.7552	0.4651	0.8299	5.2400	1.8212	0.8573
	1	1.8622	0.4959	0.8836	5.5804	1.9330	0.9131
	10	2.1356	0.5707	1.0138	6.3745	2.2229	1.0496
	∞	2.3073	0.6121	1.0907	6.8735	2.3964	1.1277
40	0	3.0182	0.8004	1.4266	8.9908	3.1343	1.4748
	0.5	3.5103	0.9302	1.6597	10.4799	3.6424	1.7147
	1	3.7245	0.9917	1.7673	11.1608	3.8661	1.8262
	10	4.2711	1.1413	2.0275	12.7489	4.4458	2.0992
	∞	4.6145	1.2243	2.1814	13.7470	4.7928	2.2554
100	0	7.5456	2.0010	3.5665	22.4771	7.8358	3.6871
	0.5	8.7758	2.3255	4.1493	26.1998	9.1059	4.2867
	1	9.3111	2.4794	4.4181	27.9021	9.6652	4.5654
	10	10.6778	2.8533	5.0688	31.8723	11.1146	5.2479
	∞	11.5363	3.0607	5.4534	34.3675	11.9821	5.6386

Table 8 represents the variation of nondimensional central deflection of ZrO_2/Ti-6Al-4V square (b/a=1) and rectangular (b/a=2) FGM plates, respectively, subjected to a uniform lateral pressure combined with a temperature rise $\Delta T = 100K$. The volume fraction index n, and side to thickness ratio a/h, is taken as 1 and 10, respectively. The load parameter p_0

TABLE VII
EFFECT OF VOLUME FRACTION INDEX n ON NONDIMENSIONAL CENTRAL DEFLECTION OF ZrO_2/Ti-6Al-4V SQUARE $(b = a)$ AND RECTANGULAR $(b = 2a)$ FGM PLATE (A/H=5) SUBJECTED TO SINUSOIDAL LOAD IN THERMAL ENVIRONMENT.

b/a	n	Boundary condition's					
		SSSS	CCCC	SCSC	CFCF	HHHH	CHCH
	0	-2.7973	-0.1153	-0.1699	-0.7415	-0.2865	-0.1758
	0.5	-3.2403	-0.1330	-0.1963	-0.8604	-0.3316	-0.2030
1	1	-3.4480	-0.1423	-0.2097	-0.9183	-0.3530	-0.2169
	10	-4.0017	-0.1675	-0.2453	-1.0629	-0.4110	-0.2543
	∞	-4.2859	-0.1770	-0.2606	-1.1361	-0.4389	-0.2697
	0	-0.6383	-0.2122	0.3410	-1.9181	-0.6670	-0.3546
	2	-0.7404	-0.2449	-0.3946	-2.2302	-0.7731	-0.4101
2	1	-0.7868	-0.2619	-0.4212	-2.3778	-0.8221	-0.4379
	10	-0.9089	-0.3072	-0.4903	-2.7350	-0.9525	-0.5107
	∞	-0.9769	-0.3254	-0.5224	-2.9353	-1.0209	-0.5433

varies from 25 to 250. As the present formulation is based on the linear variation of strain fields, hence load Verses deflection pattern is linear. It is also seen that the plates with intermediate material properties have intermediate value of deflection. The minimum deflection is observed for clamped (CCCC) and maximum value is observed for clamped-free (CFCF) boundary conditions for both square and rectangular plates.

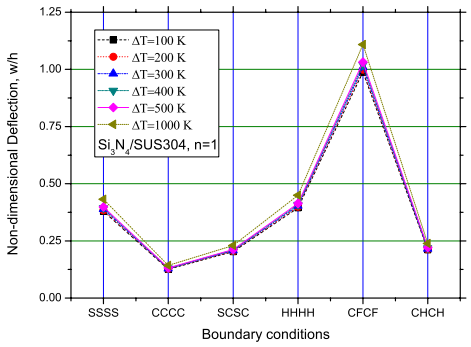

Fig. 3. Effect of temperature rise on bending behavior of square Si_3N_4/SUS304 plates subjected to uniform pressure and temperature change $(a/h$=10, n=1).

Fig. 3 shows the effect of the temperature rise on the nondimensional center deflection for plate made of Si_3N_4/SUS304 plates with different combination of boundary conditions. The temperature varies from 100 to 1000 K. The side to thickness ratio, a/h=10 and the volume fraction index, n is taken as unity. The top surface of the plate is ceramic rich, whereas the bottom surface is metal rich. A uniformly distributed load is applied on the top of the plate with loading parameter p_0=10. It can be seen that the nondimensional deflection increases as the temperature goes up. This is because the Young's modulus getting weaker when the temperature goes up. Hence, the weaker Young's modulus results in the higher deflection. The lowest and highest deflection is found for clamped (CCCC) and clamped-free (CFCF) boundary conditions, respectively.

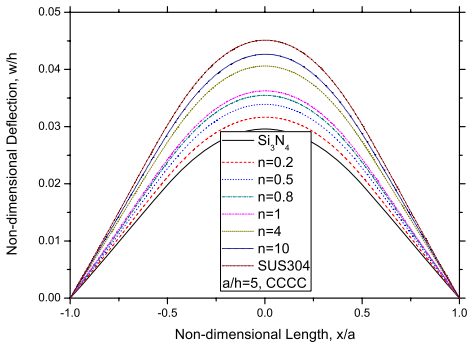

Fig. 4. Non-dimensional deflection due to uniformly applied load VS non-dimensional length for Si_3N_4/SUS304 square plate $(a/h$=5) with clamped (CCCC) boundary condition in thermal environment.

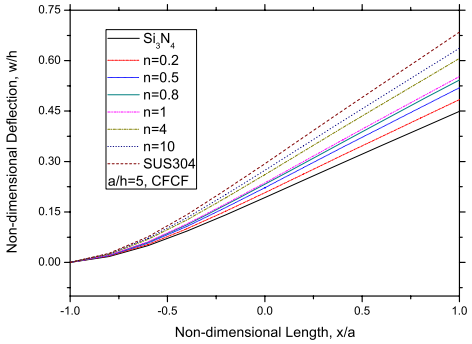

Fig. 5. Non-dimensional deflection due to uniformly applied load VS non-dimensional length for Si_3N_4/SUS304 square plate $(a/h$=5) with clamped-free (CFCF) boundary condition in thermal environment.

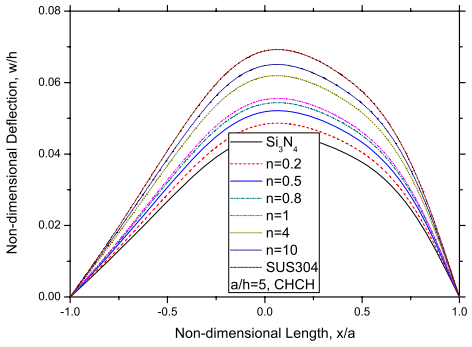

Fig. 6. Non-dimensional deflection due to uniformly applied load VS non-dimensional length for Si_3N_4/SUS304 square plate $(a/h$=5) with hinged (CHCH) boundary condition in thermal environment.

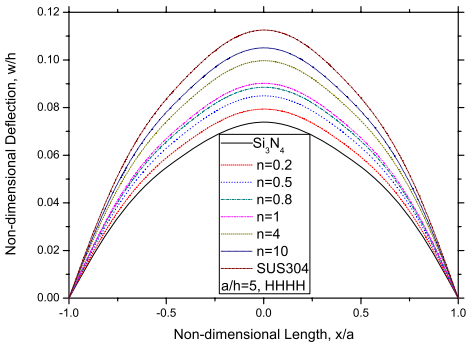

Fig. 7. Non-dimensional deflection due to uniformly applied load VS non-dimensional length for Si_3N_4/SUS304 square plate (a/h=5) with hinged (HHHH) boundary condition in thermal environment.

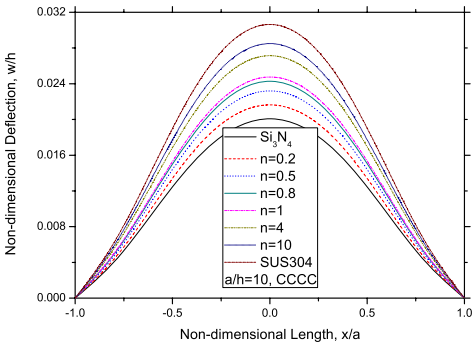

Fig. 10. Non-dimensional deflection due to uniformly applied load VS non-dimensional length for Si_3N_4/SUS304 square plate (a/h=10) with clamped (CCCC) boundary condition in thermal environment.

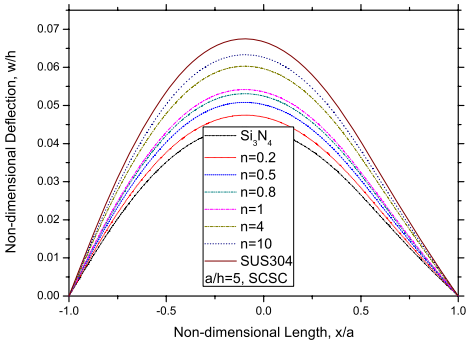

Fig. 8. Non-dimensional deflection due to uniformly applied load VS non-dimensional length for Si_3N_4/SUS304 square plate (a/h=5) with simply supported-clamped (SCSC) boundary condition in thermal environment.

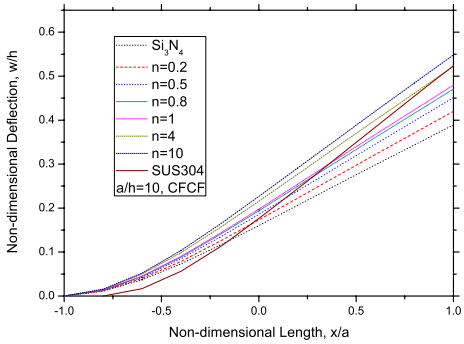

Fig. 11. Non-dimensional deflection due to uniformly applied load VS non-dimensional length for Si_3N_4/SUS304 square plate (a/h=10) with clamped-free (CFCF) boundary condition in thermal environment.

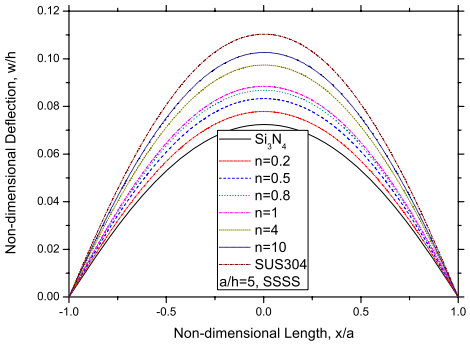

Fig. 9. Non-dimensional deflection due to uniformly applied load VS non-dimensional length for Si_3N_4/SUS304 square plate (a/h=5) with simply supported (SSSS) boundary condition in thermal environment.

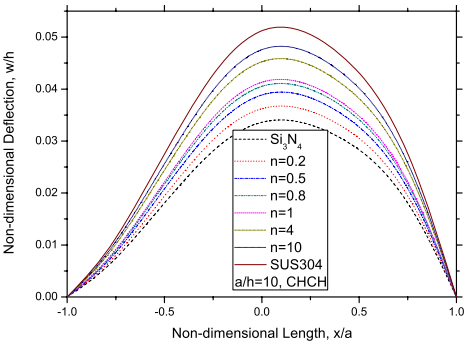

Fig. 12. Non-dimensional deflection due to uniformly applied load VS non-dimensional length for Si_3N_4/SUS304 square plate (a/h=10) with hinged (CHCH) boundary condition in thermal environment.

TABLE VIII
NONDIMENSIONAL CENTRAL DEFLECTION OF ZrO_2/TI-6AL-4V SQUARE $(b = a)$ AND RECTANGULAR $(b = 2a)$ FGM PLATE $(a/h = 10, n = 1)$ SUBJECTED TO UNIFORM PRESSURE IN THERMAL ENVIRONMENT.

b/a	p_0	Boundary condition's					
		SSSS	CCCC	SCSC	CFCF	HHHH	CHCH
1	25	0.9599	0.3190	0.5134	2.5213	0.9970	0.5326
	50	1.9197	0.6380	1.0268	5.0427	1.9939	1.0651
	75	2.8796	0.9570	1.5402	7.5640	2.9909	1.5977
	100	3.8394	1.2760	2.0536	10.0853	3.9878	2.1303
	150	5.7591	1.9140	3.0804	15.1280	5.9818	3.1954
	200	7.6788	2.5521	4.1072	20.1706	7.9757	4.2606
	250	9.5985	3.1901	5.1340	25.2133	9.9696	5.3257
2	25	2.3278	0.6198	1.1045	6.9755	2.4163	1.1414
	50	4.6556	1.2397	2.2091	13.9511	4.8326	2.2827
	75	6.9834	1.8595	3.3136	20.9266	7.2489	3.4241
	100	9.3111	2.4794	4.4181	27.9021	9.6652	4.5654
	150	13.9667	3.7191	6.6272	41.8532	14.4978	6.8481
	200	18.6223	4.9587	8.8363	55.8042	19.3304	9.1309
	250	23.2779	6.1984	11.0453	69.7553	24.1630	11.4136

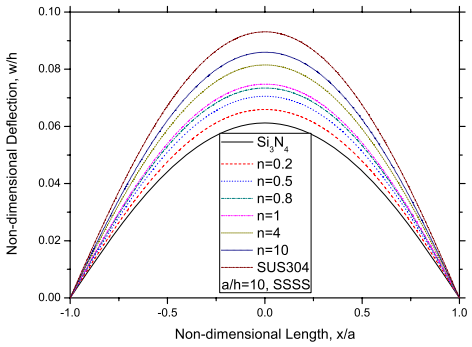

Fig. 15. Non-dimensional deflection due to uniformly applied load VS non-dimensional length for Si_3N_4/SUS304 square plate $(a/h$=10) with simply supported (SSSS) boundary condition in thermal environment.

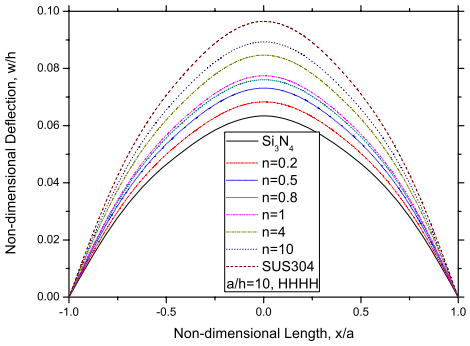

Fig. 13. Non-dimensional deflection due to uniformly applied load VS non-dimensional length for Si_3N_4/SUS304 square plate $(a/h$=10) with hinged (HHHH) boundary condition in thermal environment.

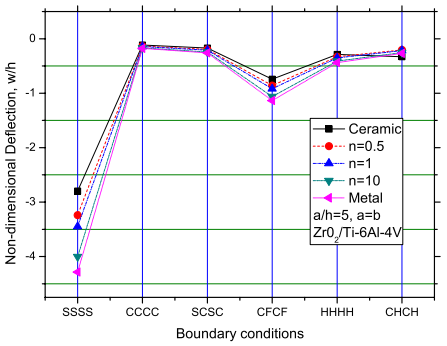

Fig. 16. Non-dimensional bending behavior of ZrO_2/Ti-6Al-4V square plate due to sinusoidal applied load with various boundary conditions in thermal environment $(a/h$=5, b/a=1).

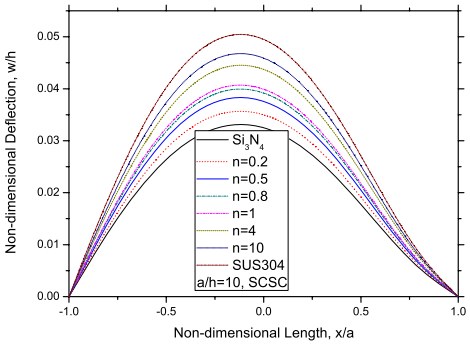

Fig. 14. Non-dimensional deflection due to uniformly applied load VS non-dimensional length for Si_3N_4/SUS304 square plate $(a/h$=10) with simply supported-clamped (SCSC) boundary condition in thermal environment.

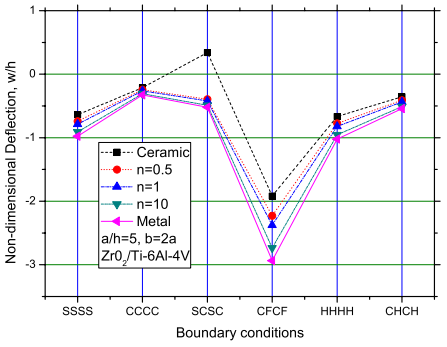

Fig. 17. Non-dimensional bending behavior of ZrO_2/Ti-6Al-4V rectangular plate due to sinusoidal applied load with various boundary conditions in thermal environment $(a/h$=5, b/a=2).

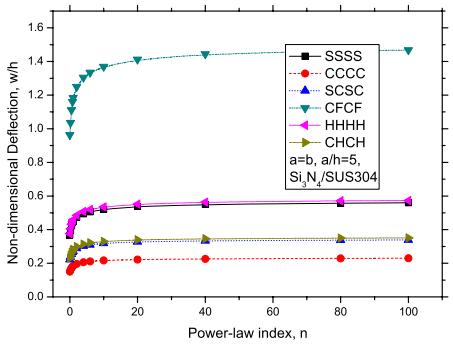

Fig. 18. Effect of volume fraction index n on non-dimensional bending behavior of Si_3N_4/SUS304 square plate due to uniformly applied load with various boundary conditions in thermal environment (a/h=5, b/a=1)

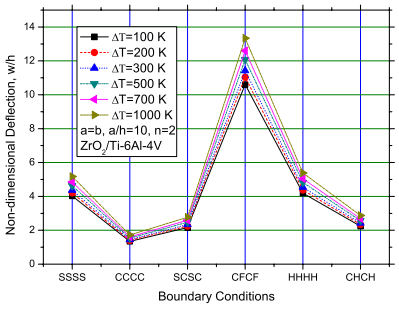

Fig. 19. Effect of temperature rise on bending behavior of square ZrO_2/Ti-6Al-4V plates subjected to uniform pressure and temperature change (a/h=10, n=2, b/a=1).

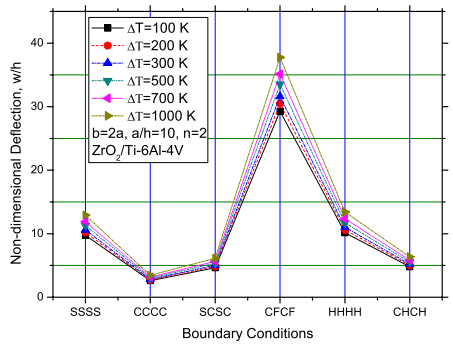

Fig. 20. Effect of temperature rise on bending behavior of rectangular ZrO_2/Ti-6Al-4V plates subjected to uniform pressure and temperature change (a/h=10, n=2, b/a=2).

Figs. 4-9 represent the nondimensional deflection VS non-dimensional length with the volume fraction index due to uniformly distributed load (p_0=10) along with a uniform temperature rise $\Delta T = 100K$ for square Si_3N_4/ SUS304 plates (a/h=5) with different combination of boundary conditions. It is perceived that the nondimensional deflection increases as the volume fraction index n increases, with the trend becoming gentler as n increases. Figs. 10-15 show the nondimensional deflection VS non-dimensional length with the volume fraction index due to uniformly distributed load (p_0=10) along with a uniform temperature rise $\Delta T = 100K$ for square Si_3N_4/ SUS304 plates (a/h=10) with different combination of boundary conditions. The nondimensional deflection behavior shown in theses figures are similar to those in figs. 5-10. It is noteworthy that when the thermal effect is induced, the mechanical response of graded plate is not necessarily intermediate to that of isotopic metal and the ceramic plate. As shown in fig. 11, the deflection of the graded plate with n=4 is not intermediate with other values of volume fraction index n. Figs. 16-17 represent nondimensional bending behavior of square and rectangular ZrO_2/Ti-6Al-4V FGM plates (a/h=5), respectively with varying volume fraction index n and under two types of loading conditions. The plates are subjected to sinusoidal load combined with a temperature rise $\Delta T = 100K$. It is found that the maximum deflection is observed for simply supported boundary condition (SSSS) for square plate, and consequently in the case of rectangular plate (b=2a) same is found for clamped-free (CFCF) boundary condition.

Fig. 18 shows the comparison of the nondimensional deflection, by varying the volume fraction indices, n due to uniformly distributed load (p_0=10) along with a temperature rise $\Delta T = 100K$ for square Si_3N_4/SUS304 plates ($a/h = 5$) with different combination of boundary conditions. It can be seen that all of the curves that represent the various combinations show the similar behavior with the deflection increases as the volume fraction index n increases, nearly around $n = 20$. The deflection is approximately insensitive after $n \geq 20$. Figs. 19-20 represent the effect of the temperature on the nondimensional center deflection for square and rectangular plates, respectively, made up of ZrO_2/Ti-6Al-4V with different combination of boundary conditions. The temperature varies from 100 to 1000 K. The plates are subjected to uniform distributed load with load parameter p_0=100. The side to thickness ratio a/h=10, and volume fraction index $n = 2$. It is found that least deflection is reported for clamped (CCCC) condition and maximum is found in clamped-free (CFCF) type of boundary condition for both square and rectangular plates.

VI. Concluding Remarks

Thermo-mechanical deformations of functionally graded ceramic-metal plates under various loading and boundary conditions is investigated. The analysis is carried out using the higher order shear deformation theory with an admissible alteration in the transverse displacements in conjunction with finite element models. The systems of algebraic equations are derived using variational approach, and a C^0 continuous isoparametric Lagrangian element with 13 DOFs per node is developed and implemented in the said problem. Convergence tests and validation studies have been carried out to inculcate the credibility of the present formulation. The obtained result shows a good agreement with those available in the literature.

It is observed that, when thermal effect is induced, the bending response of the functionally graded plate is not necessarily intermediate to those of the metal and the ceramic plate. This behavior is found to be true irrespective of boundary conditions. The temperature dependent material properties should be taken into account for accurate analysis in high temperature applications. Numerical results for different volume fraction indices, the aspect ratios, the thickness ratios, the temperature rise along with different combinations of the loading and boundary conditions have been presented.

ACKNOWLEDGEMENT

The authors gratefully acknowledge the financial support provided by the All India Council for Technical Education (AICTE), New Delhi, INDIA. (F. No: 1-10/RID/NDF-PG(19)/2008-09, Dated 13^{th} March 2009.) A statutory body of the Government of INDIA.

REFERENCES

[1] M. Koizumi, The concept of FGM, *Proceedings of the Second International symposium on*FGM, vol. 34, pp. 3−10, 1993.
[2] M. Koizumi, FGM activities in Japan, *Composites Part B*, vol. 28B, pp. 1−4, 1997.
[3] E. Reissner,The Effect of transverse shear deformation on the bending of elastic plates, *J. appl. Mech.*, vol. 12 Trans, A69−A77, 1945.
[4] Mindlin, R. D. Influence of rotatory inertia and shear on flexural vibrations of isotropic elastic plates, *J. Appl. Mech.,* vol. 73, pp. 31−38, 1951.
[5] R. B. Nelson, and D. R. Larch, A refined theory of laminated orthotropic plates, *J. appl. Mech.*, vol. 41, pp. 177-183, 1974.
[6] Reissner, E. On Transverse bending of plates including the effect of transverse shear deformation., *Int. J. Solids Struct.*, 1975, 11, 569-573.
[7] K. H. Lo, R. M. Christensen, and E. M. Wu, A high-order theory of plate deformation-part I: homogeneous plates., *J. appl. Mech.*, vol. 44, pp.663-668, 1977.
[8] J. N. Reddy, A simple higher-order theory for laminated composite plates. *J. appl. Mech*, vol.51, pp. 745-752,1984.
[9] J. N. Reddy, Analysis of functionally graded plates, *Int. J. Numer. Method Engng.,* vol.47, pp. 663−684, 2000.
[10] S. Abrate, Free vibration buckling and static deflections of functionally graded plates, *Compos. Scie. and Tech.,* vol. 66, pp.2383−2394, 2006.
[11] PARK, Jae-Sang. and KIM, Ji-Hwan. Thermal postbuckling and vibration analyses of functionally graded plates,*J. Sound vibr*., vol. 289, pp.77−93, 2006.
[12] Wu. Lanhe, Thermal buckling of a simply supported moderately thick rectangular FGM plate, *Compo. Struct*., vol. 64, pp. 211−218, 2004.
[13] A. R. Saidi, and E. Jomehzadeh, On the analytical approach for the bending/stretching of linearly elastic functionally graded rectangular plates with two opposite edges simply supported, *Proc. IMechE, Part C*., 2009, 223, 1873−1884.
[14] Wu. Lanhe, Thermal buckling of a simply supported moderately thick rectangular FGM plate,*Compo. Struct.*, vol. 64, pp.211−218, 2004.
[15] A. J. M, Ferreira, R.C, Batra, C.M.C, Roque, L.F, Qian, and P.A.L.S, Martins, Static analysis of functionally graded plates using third order shear deformation theory and a meshless method,*Compo. Struct.*, vol. 69, pp. 449−457, 2005.
[16] J. Yang, and H. S. Shen,Vibration characteristics and transient response of shear-deformable functionally graded plates in thermal environments, *J. Sound Vibr.*, vol. 255, pp. 579−602, 2000.
[17] L.F, Qian. R. C. Batra, and L. M. Chen, Static and dynamic deformations of thick functionally graded elastic plates by using higher order shear and normal deformable plate theory and meshless local Petrov-Galerkin method , *Composite Part B*, pp.685−697, 2004.
[18] E. Efraim,a nd M. Eisenberger, Exact vibration analysis of variable thickness annular isotropic and FGM plates, *J. Sound Vibr.*, vol. 299, pp. 720−738, 2007.
[19] M. H. Naei, A. Masoumi, and A. Shamekhi, Buckling analysis of circular functionally graded material plate having variable thickness under uniform compression by finite-element method,*Proc. IMechE, Part C*, vol. 221 pp. 1241−1247, 2007.
[20] H. M. Navazi, and H. Haddadpour, Aero-thermoelastic stability of functionally graded plates, *Compos. Struct.*, vol. 80, pp. 580−587, 2007.
[21] J. N. Reddy, and Z. Q. Cheng, Frequency of functionally graded plates with three-dimensional asymptotic approach, *J. of Engg. Mech.*, vol. 129 (8), pp. 896−900, 2003.
[22] T. M. Nguyen, K. Sab, and G. Bonnet, First-order shear deformation plate models for functionally graded materials,*Compos. Struct.*, vol. 83, pp. 25−36, 2008.
[23] K. M. Liew, K. C. Hung, and M. K. Lim, A continuum three-dimensional vibration analysis of thick rectangular plates, *Int. J. Solids Struct.*, vol. 30 (24), pp. 3357−3379, 1993
[24] H. Matasunaga, Analysis of functionally graded plates, *Compos. Struct.*, vol. 82, pp. 499−512, 2008.
[25] Y. S. Touloukian, Thermophysical properties of high temprature solid materials., MacMillan, New York, 1967.
[26] X.I. Huang, and H. S. Shen, Nonlinear vibration and dynamic response of functionally graded plates in thermal environments *Int. J. Solids and Struct.*, vol. 41, pp. 2403-2427, 2004.
[27] Mohammad Talha, B. N. Singh, "Static response and free vibration analysis of FGM plates using higher order shear deformation theory," *App. Math. Model.,* vol. 34, pp. 3991-4011, 2010.